Supplementary Information for

Polyoxometalate-assisted crystallization for ultraselective Ln(III)/An(VI) separation under strongly acidic conditions

Guangtao Zhang[a], Yarui Li[a], Jiarui Chen[a], Yunyi Cui[a], Xiaoyuan Zhou[b], Qing Zou[b], Xiaofeng Guo[c], Yongxin Li[d], Peng Lin[b,*], and Jian Lin[a,*]

[a] *School of Nuclear Science and Technology, Xi'an Jiaotong University, Xi'an 710049, PR China. *jianlin@xjtu.edu.cn*

[b] *Department of Radioactive Waste Technology and Radiochemistry Research, China Nuclear Power Technology Research Institute Co., Ltd., Shenzhen 518124, P.R. China. *lin_peng@cgnpc.com.cn*

[c] *Department of Chemistry and Alexandra Navrotsky Institute for Experimental Thermodynamics, Washington State University, Pullman, WA 99164-4630, USA.*

[d] *Division of Chemistry and Biological Chemistry, School of Physical and Mathematical Sciences, Nanyang Technological University, 637371, Singapore*

Table of Contents

Supplementary Figures

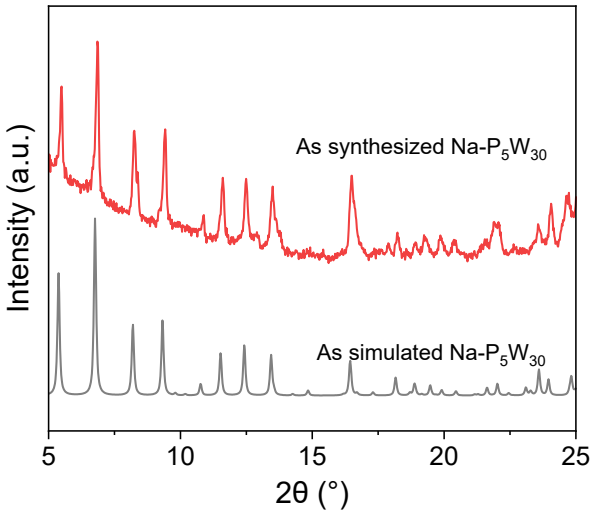

Fig. S1. PXRD patterns of simulated and as-synthesized Na-P_5W_{30}.

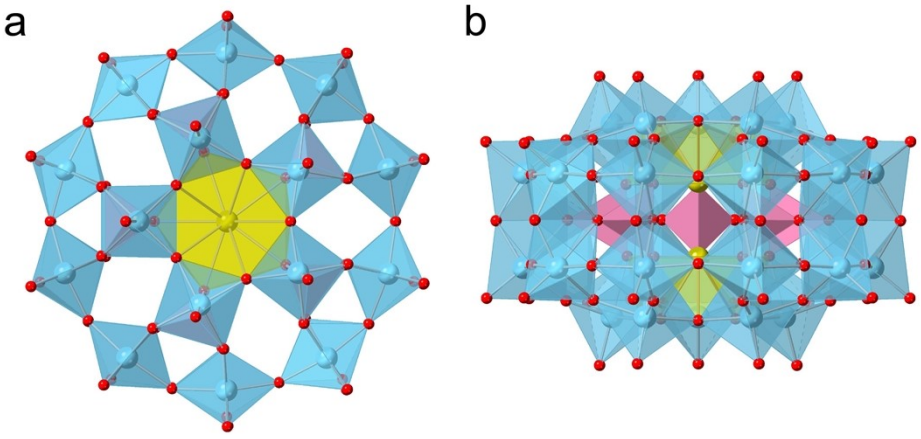

Fig. S2. Structure of $[NaP_5W_{30}O_{110}]^{14-}$ viewed (a) along and (b) perpendicular to the C_5 rotational axis. Color code: O in red, Na in yellow, P in light rose, and W in pale cyan.

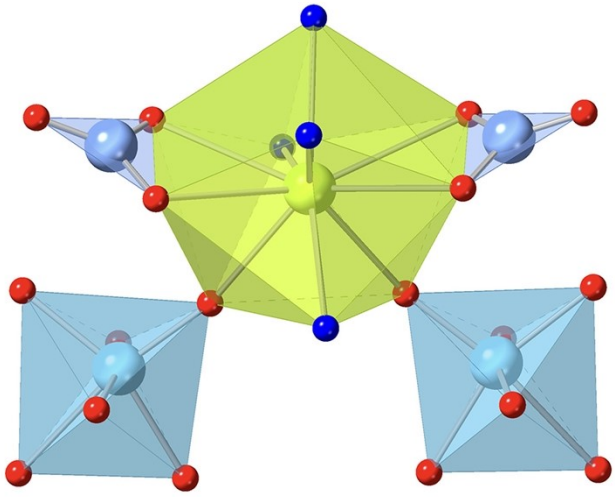

Fig. S3. Coordination geometry of lanthanide cations in Ln-P_5W_{30}-1. Color code: Ln in chartreuse, N in pale blue, W in pale cyan, O from NO_3^- or WO_6 in red, and O from H_2O in blue.

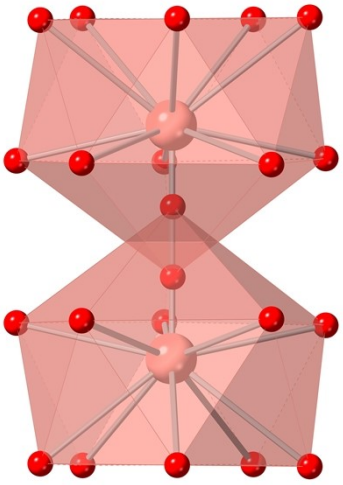

Fig. S4. Coordination geometry of lanthanide cations in Ln-P_5W_{30}-2. Color code: O in red, Ln in orange.

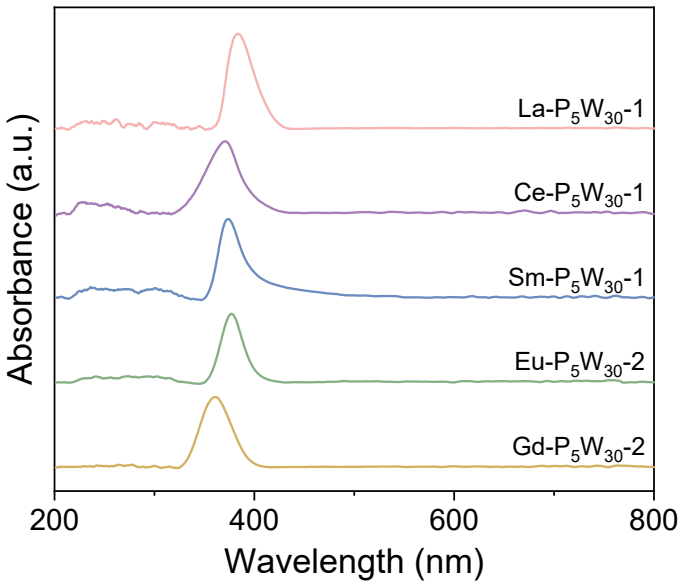

Fig. S5. Solid-state UV-vis absorption spectra obtained from single crystals of Ln-P_5W_{30}-1 and Ln-P_5W_{30}-2.

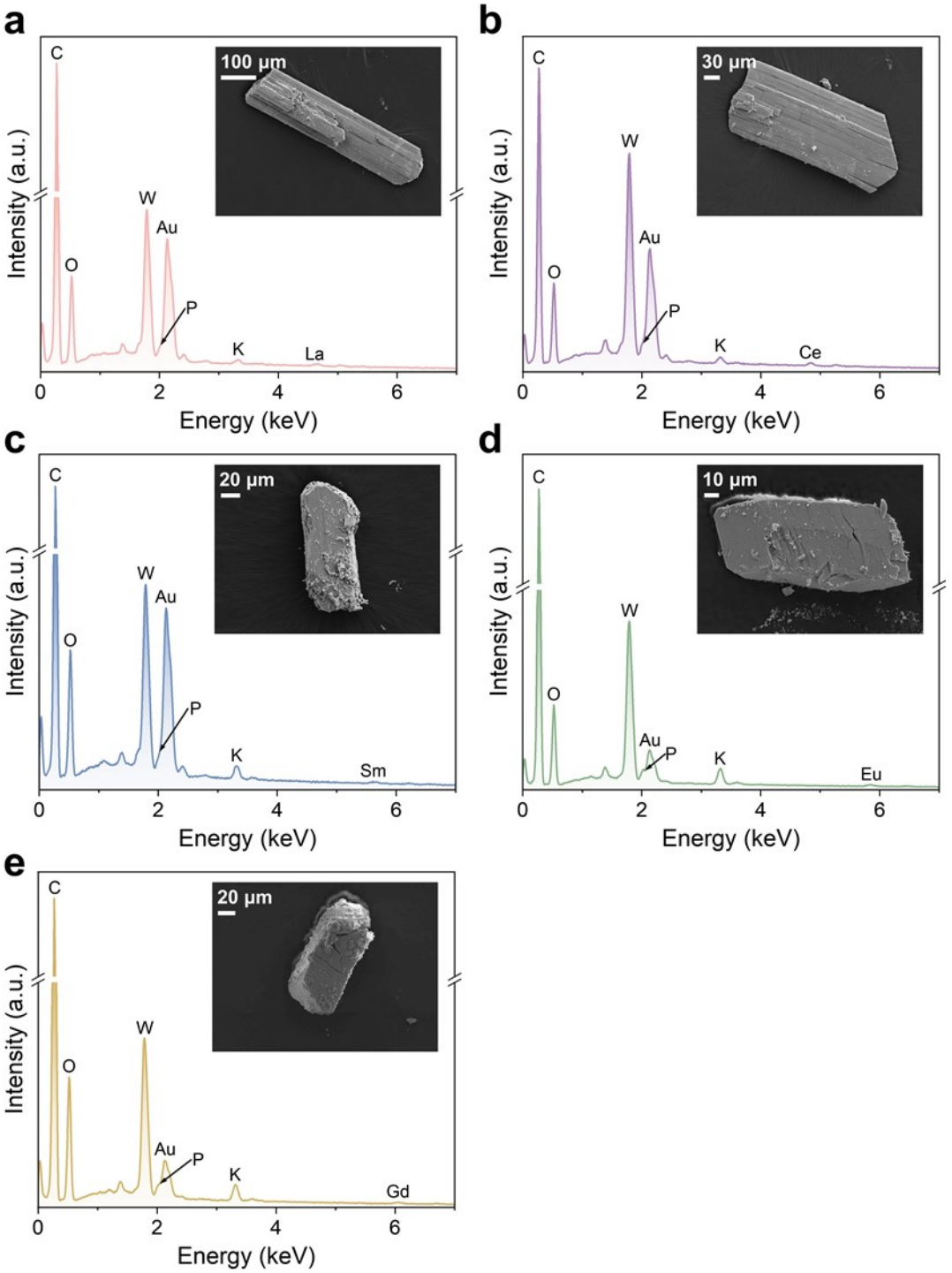

Fig. S6. SEM images and EDS spectra of (a) La-P_5W_{30}-1, (b) Ce-P_5W_{30}-1, (c) Sm-P_5W_{30}-1, (d) Eu-P_5W_{30}-2, and (e) Gd-P_5W_{30}-2, prepared by reactions of $Ln(NO_3)_3 \cdot 6H_2O$ with Na-P_5W_{30} in 0.3 M HNO_3.

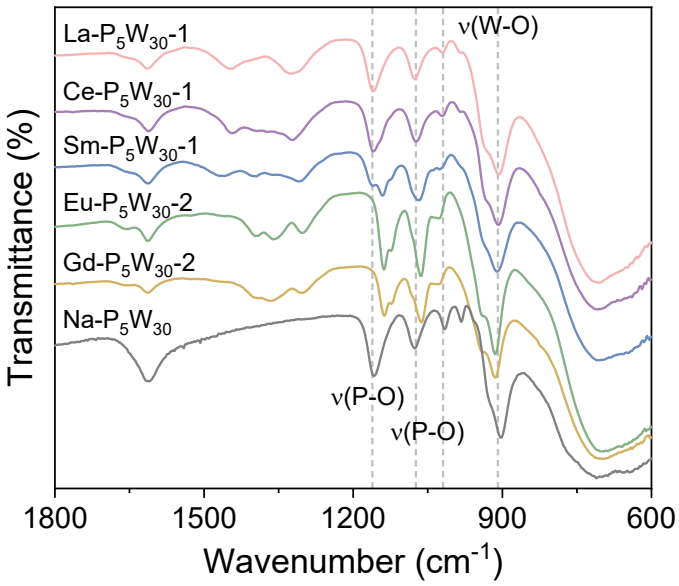

Fig. S7. FT-IR spectra Ln-P_5W_{30}-1 and Ln-P_5W_{30}-2 prepared by reactions of $Ln(NO_3)_3 \cdot 6H_2O$ with Na-P_5W_{30} in 0.3 M HNO_3 in comparison with that of Na-P_5W_{30}.

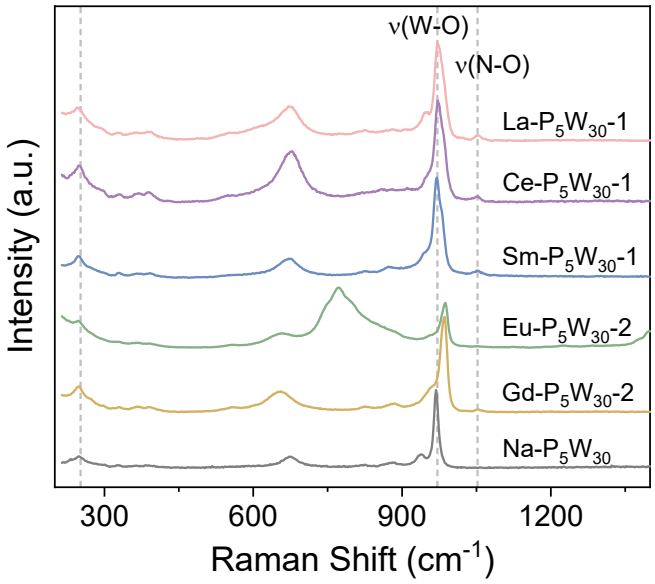

Fig. S8. Raman spectra of Ln-P_5W_{30}-1 and Ln-P_5W_{30}-2 prepared by reactions of $Ln(NO_3)_3 \cdot 6H_2O$ with Na-P_5W_{30} in 0.3 M HNO_3 in comparison with that of Na-P_5W_{30}.

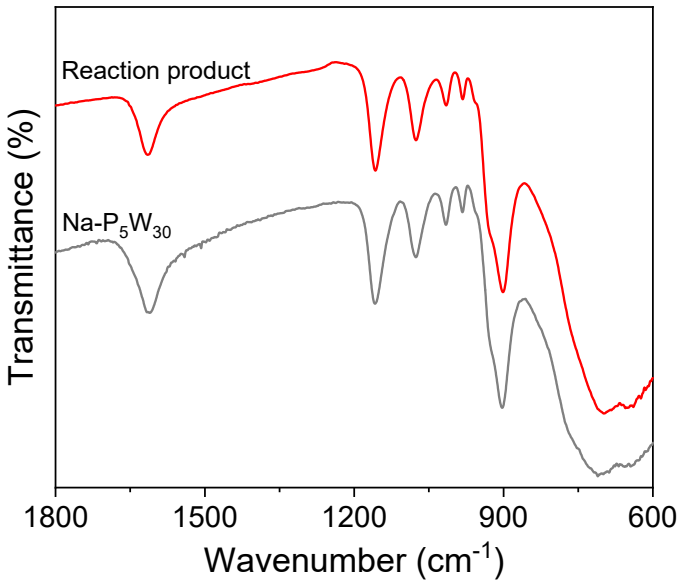

Fig. S9. FT-IR spectra of Na-P_5W_{30} and the reaction product of Na-P_5W_{30} with $UO_2(NO_3)_2 \cdot 6H_2O$ in 0.3 M HNO_3.

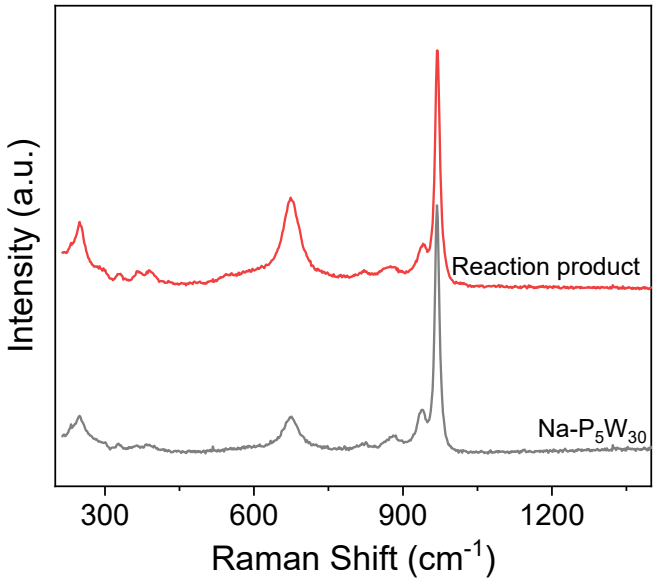

Fig. S10. Raman spectra of Na-P_5W_{30} and the reaction product of Na-P_5W_{30} with $UO_2(NO_3)_2 \cdot 6H_2O$ in 0.3 M HNO_3.

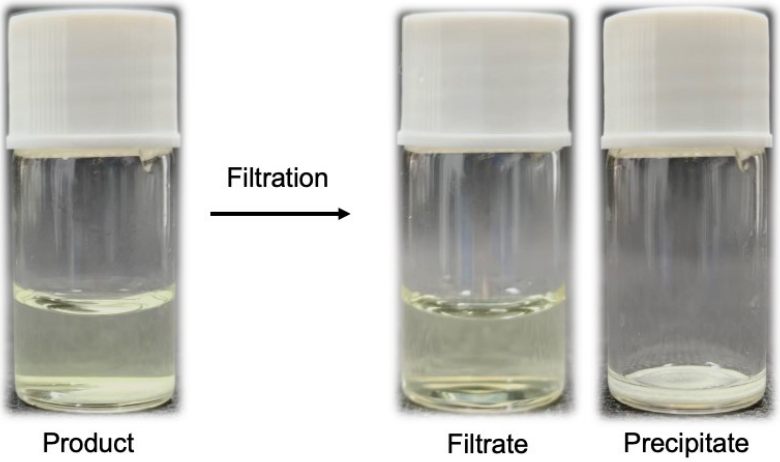

Fig. S11. Photographs showing the colors of the filtrate and solid product after reaction of $UO_2(NO_3)_2 \cdot 6H_2O$ with Na-P_5W_{30} in 0.3 M HNO_3.

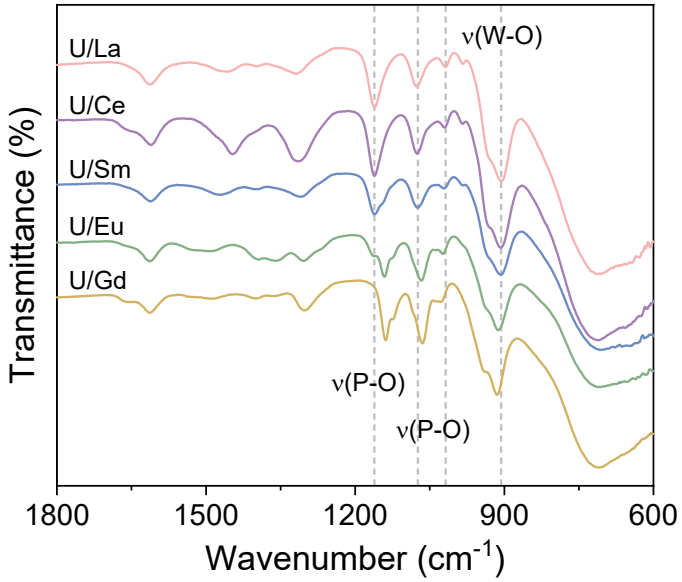

Fig. S12. FT-IR spectra of solid-phase products obtained by selective crystallization from binary Ln(III)/U(VI) systems (Ln = La, Ce, Sm, Eu, and Gd) in 0.3 M HNO_3.

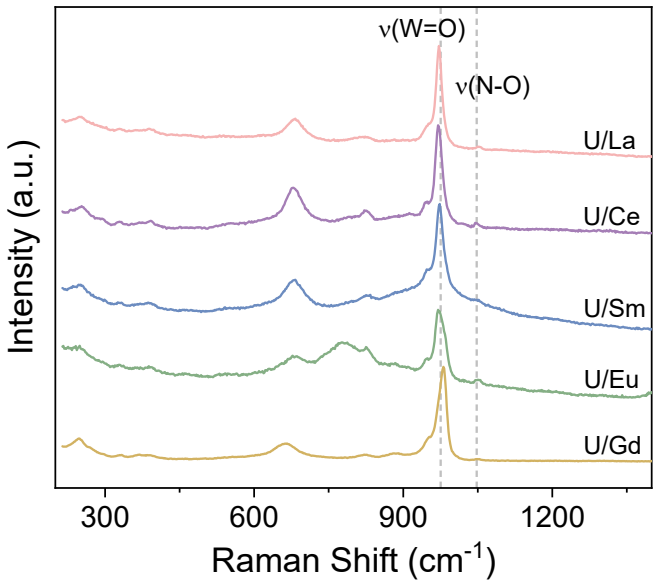

Fig. S13. Raman spectra of solid-phase products obtained by selective crystallization from binary Ln(III)/U(VI) systems (Ln = La, Ce, Sm, Eu, and Gd) in 0.3 M HNO_3.

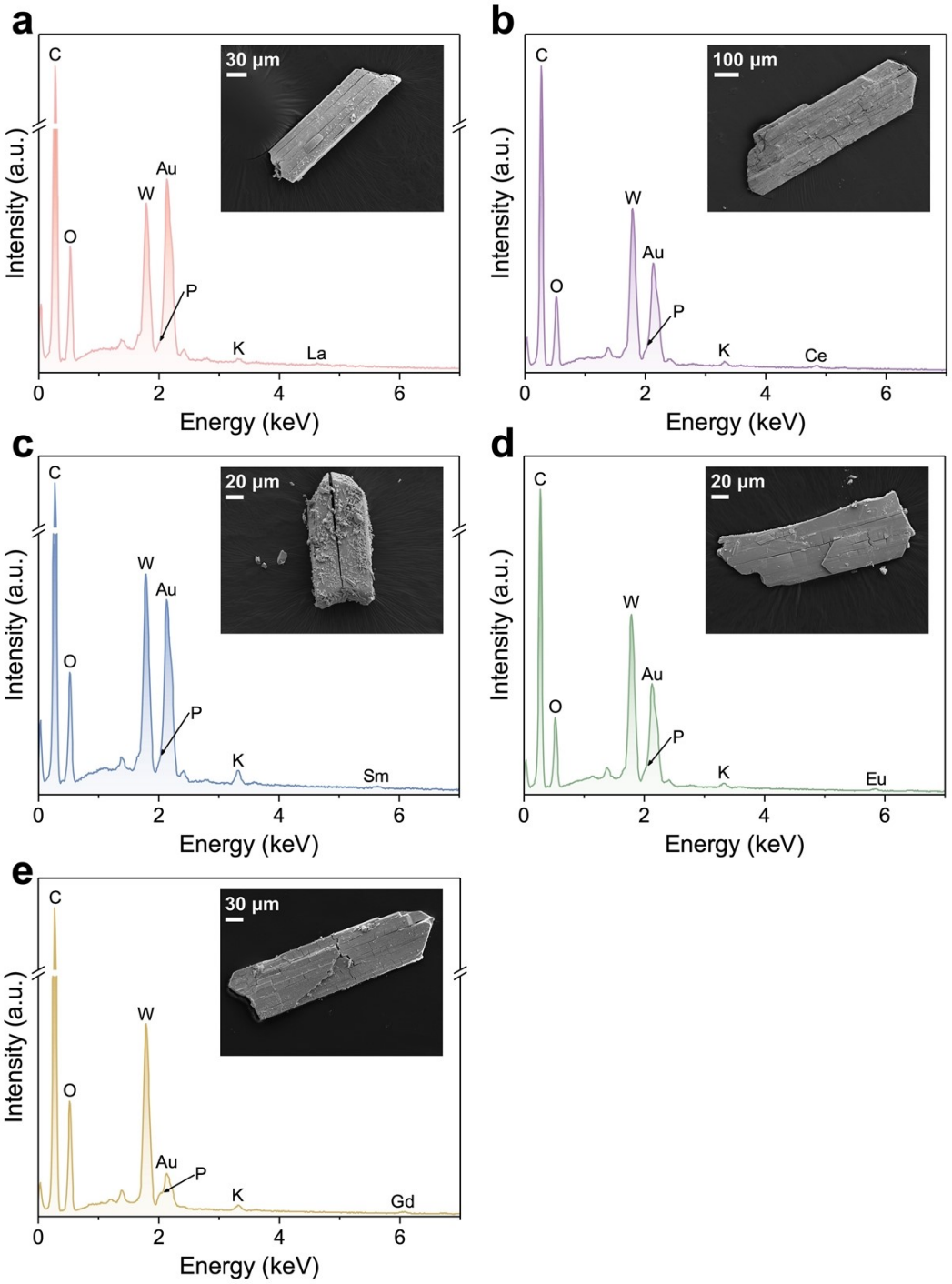

Fig. S14. SEM images and EDS spectra of (a) La-P_5W_{30}-1, (b) Ce-P_5W_{30}-1, (c) Sm-P_5W_{30}-1, (d) Eu-P_5W_{30}-1, and (e) Gd-P_5W_{30}-1, prepared by reactions of $Ln(NO_3)_3 \cdot 6H_2O$ with Na-P_5W_{30} in 3 M HNO_3.

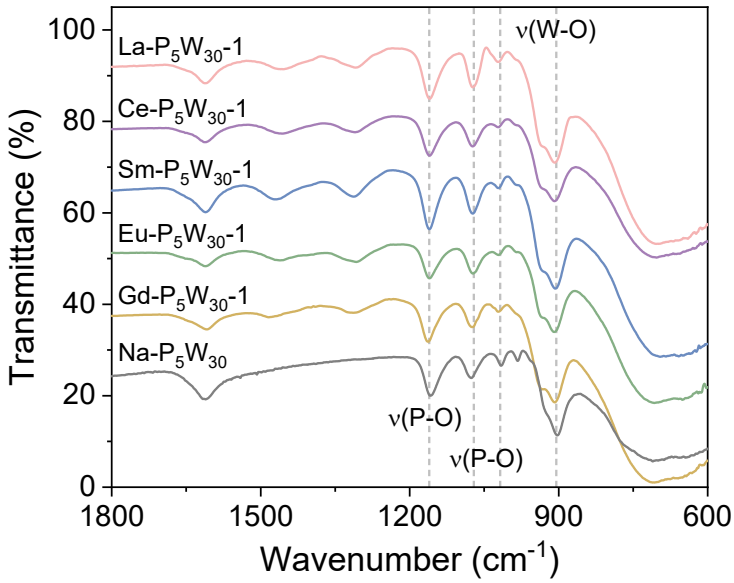

Fig. S15. FT-IR spectra of Ln-P_5W_{30}-1 and Ln-P_5W_{30}-2 prepared by reactions of $Ln(NO_3)_3 \cdot 6H_2O$ with Na-P_5W_{30} in 3 M HNO_3 in comparison with that of Na-P_5W_{30}.

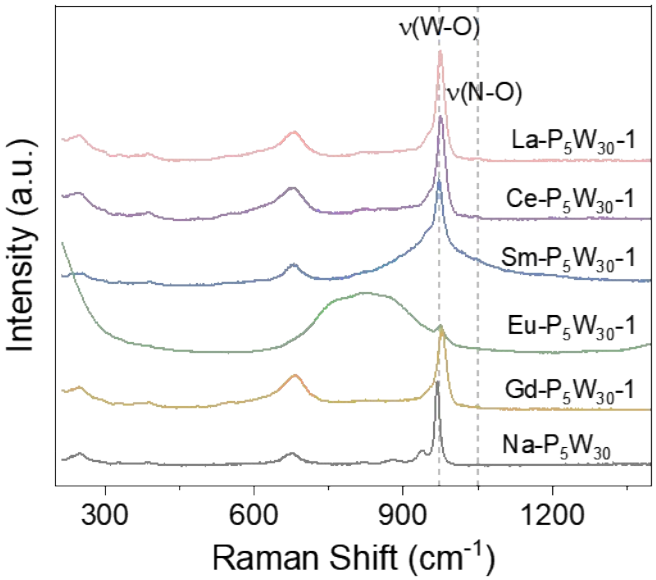

Fig. S16. Raman spectra of Ln-P_5W_{30}-1 and Ln-P_5W_{30}-2 prepared by reactions of $Ln(NO_3)_3 \cdot 6H_2O$ with Na-P_5W_{30} in 3 M HNO_3 in comparison with that of Na-P_5W_{30}.

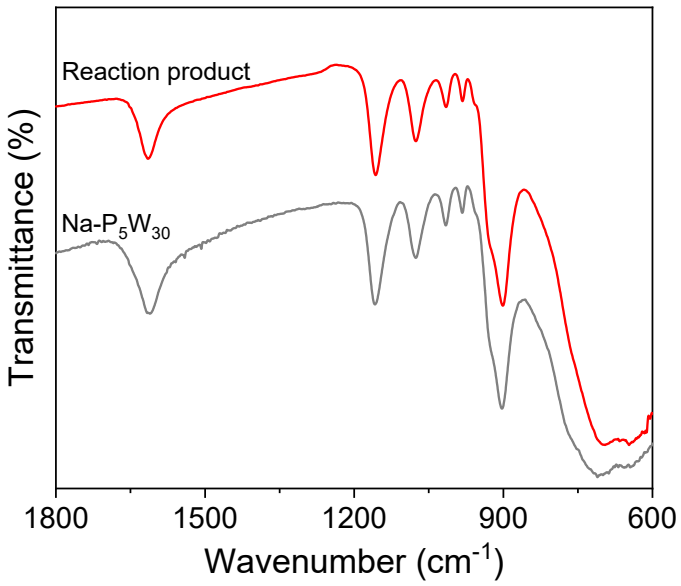

Fig. S17. FT-IR spectra of $Na\text{-}P_5W_{30}$ and the reaction product of $Na\text{-}P_5W_{30}$ with $UO_2(NO_3)_2{\cdot}6H_2O$ in 3 M HNO_3.

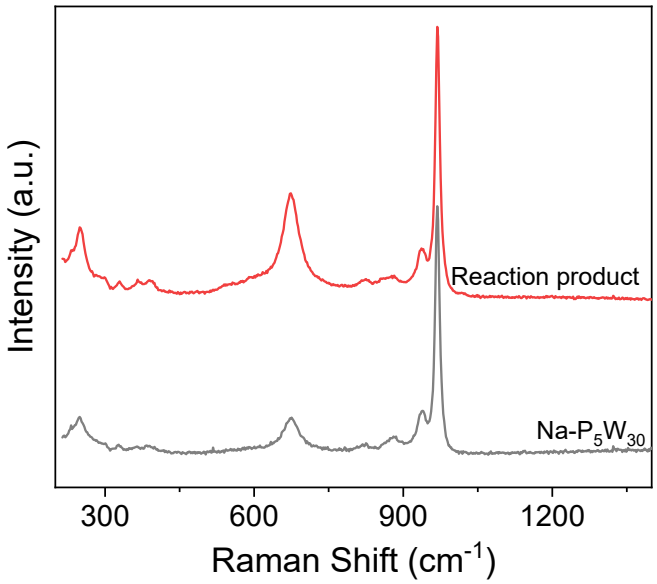

Fig. S18. Raman spectra of $Na\text{-}P_5W_{30}$ and the reaction product of $Na\text{-}P_5W_{30}$ with $UO_2(NO_3)_2{\cdot}6H_2O$ in 3 M HNO_3.

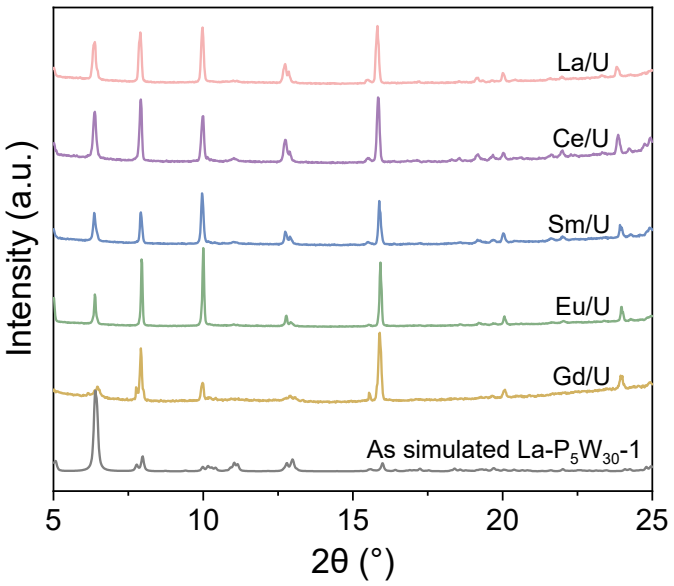

Fig. S19. PXRD patterns of the solid-phase products obtained by selective crystallization from binary Ln(III)/U(VI) systems (Ln = La, Ce, Sm, Eu, and Gd) in 3 M HNO_3, compared with the simulated pattern of La-P_5W_{30}-1.

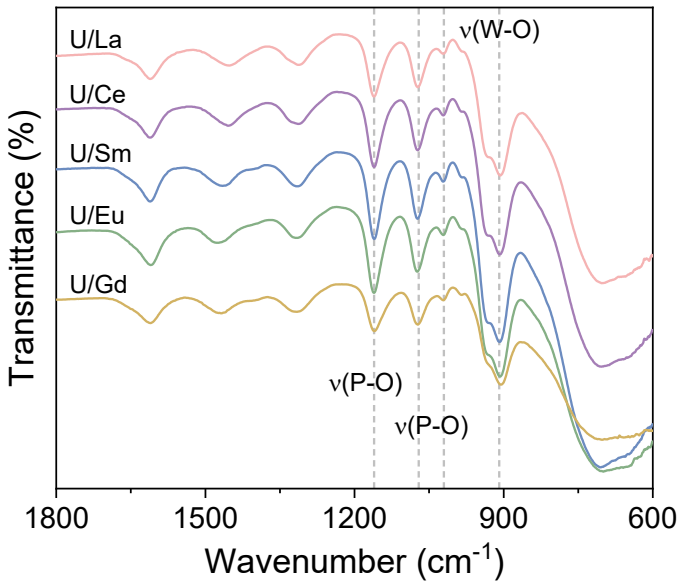

Fig. S20. FTIR spectra of the solid-phase products obtained by selective crystallization from binary Ln(III)/U(VI) systems (Ln = La, Ce, Sm, Eu, and Gd) in 3 M HNO_3.

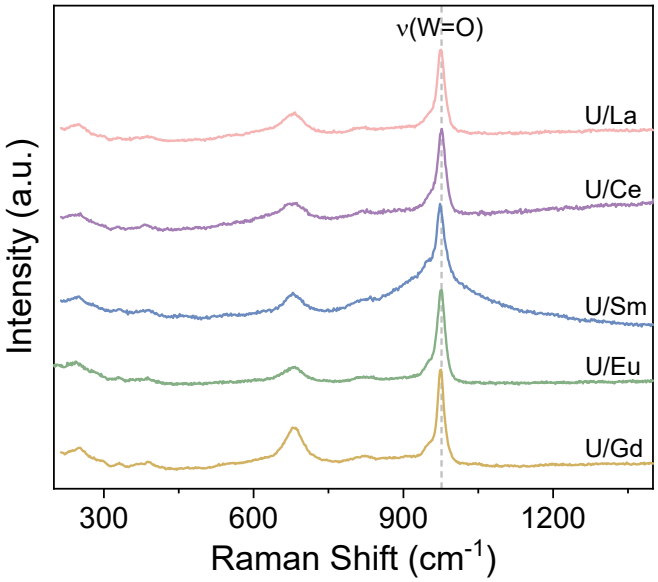

Fig. S21. Raman spectra of the solid-phase products obtained by selective crystallization from binary Ln(III)/U(VI) systems (Ln = La, Ce, Sm, Eu, and Gd) in 3 M HNO_3.

Supplementary Tables

Table S1. Crystallographic data for Ln-P_5W_{30}-1 (La, Ce, Sm, and Eu) and Ln-P_5W_{30}-2 (Gd).

Compound	La-P_5W_{30}-1	Ce-P_5W_{30}-1	Sm-P_5W_{30}-1	Eu-P_5W_{30}-1	Gd-P_5W_{30}-2
CCDC number	2422242	2522240	2522243	252241	252244
Formula	$K_6H_{44}La_2NaN_4O_{141}P_5W_{30}$	$K_6H_{46}Ce_2NaN_4O_{142}P_5W_{30}$	$K_6H_{45.72}Sm_{2.14}Na_{0.86}N_4O_{142}P_5W_{30}$	$K_4H_{26}Eu_2Na_3N_4O_{132}P_5W_{30}$	$K_5H_{46}GdNa_2NO_{133}P_5W_{30}$
Formula weight	8564.88	8582.32	8620.41	8393.60	8257.20
$\rho_{calc.}$ (g cm^{-3})	4.086	4.090	4.157	4.038	4.467
μ (mm^{-1})	25.762	25.775	26.284	26.150	29.033
Color	colorless	colorless	colorless	colorless	colorless
Space group	$P2_1/m$	$P2_1/m$	$P2_1/m$	$P2_1/m$	$P2_1/m$
a (Å)	17.774(2)	17.792(3)	17.709(2)	17.688(2)	16.4243(17)
b (Å)	22.008(2)	21.961(3)	21.906(3)	22.029 (2)	21.376(2)
c (Å)	18.0692(19)	18.126(3)	18.0279(18)	18.014(2)	17.499(2)
α (deg)	90	90	90	90	90
β (deg)	104.629(4)	101.839(5)	101.690(4)	101.361(5)	96.475(5)
γ (deg)	90	90	90	90	90
V (Å^3)	6923.2(14)	6932.0(18)	6848.5(14)	6881.5(14)	6104.6(11)
Z	2	2	2	2	2
T (K)	150.0	150.0	150.0	150.0	150.0
λ (Å)	0.71073	0.71073	0.71073	0.71073	0.71073
Max 2θ (deg)	55.028	54.968	55.016	54.96	54.97
R_1	0.0487	0.0475	0.0435	0.0594	0.0927
wR_2	0.1253	0.0991	0.0923	0.1467	0.2558
R_{int}	0.1173	0.0935	0.1432	0.1304	0.1610
GooF	1.056	1.036	1.022	1.039	1.042

Table S2. Comparison of An(VI)/Ln(III) separation factors (SFs) for solid-phase separation methods, including adsorption and selective crystallization reported in the literature, as well as the selective crystallization demonstrated in this work.

Separation method	Materials or crystallization ligands	SF	Acidity	Ref.
Adsorption	1f	99	pH=3	[1]
	BNNSs-DAPhen	196	5 M HNO_3	[2]
	BCN-DAPhen	592	5 M HNO_3	[3]
	HfP-0.80	696	0.1 M HNO_3	[4]
	4e	1144	pH=3	[1]
	SBA-15-ABDMA	1293	pH=3	[5]
	T-DOPOR	1543	pH=2	[6]
	DAPhen-COF	5170	0.5 M HNO_3	[7]
	BIMB	10010	pH=3	[8]
	3c	14082	pH=3	[1]
	4d	116140	pH=3	[1]
Selective crystallization	Se_6W_{45}	1100	0.1 M HNO_3	[9]
	P_5W_{30}	41139	3 M HNO_3	**This work**
	NMP	402	3 M HNO_3	[10]
	L2	6571	0.5 M HNO_3	[11]
	IDRET	48586	pH=3	[12]
	NMP	201700	1.5 M HNO_3	[10]
	L2	756276	0.08 M CH_3COOH	[13]

1f: N'1, N'4-bis((E)-pyridin-2-ylmethylene)terephthalohydrazide. BNNSs–DAPhen: Boron nitride nanosheets-diamide phenanthroline. BCN–DAPhen: Phenanthroline diamide functionalized porous carbon doped boron nitride. 4e: (E)-2-hydroxy-N'-(pyrimidin-2-ylmethylene)benzohydrazide. T-DOPOR: Modified cellulose microspheres. BIBM: 1,4–bis(imidazol–1–ylmethyl)benzene. 3c: (E)-N'-(2-hydroxybenzylidene)benzohydrazide. 4d: (E)-N'-(2-hydroxybenzylidene)picolinohydrazide. NMP: N-methyl 2-pyrrolidone. L2: (E)-N′-(pyridin-2-ylmethylene) picolinohydrazide.

Supplementary References

[1] J. Wang, R. Yao, Y. Li, Z. Lu, B. Yang, Z. Wu, Y. Li, J. Zeng, Z. Geng and Z. Wang, Planar-coordination-induced precipitation by hydrazone-bridged clusters enables uranium–rare earth separation and high-purity uranium recovery from nuclear wastewater, *J. Hazard. Mater.*, 2025, **499**, 140233.

[2] G. Chen, H. Weng, Z. Wu, Y. Chen, P. Zhang, G. Ye and M. Lin, High-yield production of monolayer boron nitride nanosheets by cationic-surfactant-assisted solvothermal exfoliation for the ultrafast and selective separation of U(VI) from lanthanides, *Sep. Purif. Technol.*, 2021, **278**, 119645.

[3] Y. Chen, P. Zhang, L. Jiao, G. Chen, Y. Yang, H. Chong and M. Lin, High efficient and selective removal of U(VI) from lanthanides by phenanthroline diamide functionalized carbon doped boron nitride, *Chem. Eng. J.*, 2022, **446**, 137337.

[4] L.-p. Xiong, K. Lv, M. Gu, C.-t. Yang, F.-c. Wu, J. Han and S. Hu, Efficient capture of actinides from strong acidic solution by hafnium phosphonate frameworks with excellent acid resistance and radiolytic stability, *Chem. Eng. J.*, 2019, **355**, 159-169.

[5] F. Zhang, Y. Liu, K.-Q. Ma, H. Yan, Y. Luo, F.-C. Wu, C.-T. Yang, S. Hu and S.-M. Peng, Highly selective extraction of uranium from wastewater using amine-bridged diacetamide-functionalized silica, *J. Hazard. Mater.*, 2022, **435**, 129022.

[6] D. Wen, C. Xie, Z. Dong, M. Zhang, M. Zhai and L. Zhao, Facile preparation of novel DOPO functionalized cellulose microspheres with superior selectivity for U(VI) from lanthanides, *Sep. Purif. Technol.*, 2022, **301**, 121969.

[7] R.-J. Cao, H.-Y. Zhou, Q.-Y. Wu, Z. Xiao, T.-Y. Xiu, J. Li, H.-B. Tang, L.-Y. Yuan, W.-S. Wu and W.-Q. Shi, Rigidity-Flexibility Regulation and Hard-Soft Donor Combination: Dual Strategies in Covalent Organic Frameworks Construction for Actinides/lanthanides Separation, *Adv. Mater.*, 2025, **37**, 2414659.

[8] R. Yao, Y. Li, J. Wang, B. Yang, Z. Wu, Y. Li, Z. Lu, J. Zeng, Z. Geng and Z. Wang, Efficient Uranium/Lanthanides Separation from Nuclear Waste via Supramolecular Self-Assembly of Flexible Molecule: High Capacity, Selectivity, and Fast Recovery, *Adv. Funct. Mater.*, 2025, e22094.

[9] H. Zhang, A. Li, K. Li, Z. Wang, X. Xu, Y. Wang, M. V. Sheridan, H.-S. Hu, C. Xu, E. V. Alekseev, Z. Zhang, P. Yan, K. Cao, Z. Chai, T. E. Albrecht-Schönzart and S. Wang, Ultrafiltration separation of Am(VI)-polyoxometalate from lanthanides, *Nature*, 2023, **616**, 482-487.

[10] X. Yin, Y. Wang, X. Li, J. Xie, M. A. Silver, L. Chen, D. Sheng, G. Ji, Z. Chai and S. Wang, Competing Crystallization between Lanthanide and Actinide in Acidic Solution Leading to Their Efficient Separation, *Chin. J. Chem* . 2019, **37**, 53-57.

[11] Y. Li, G. Zhang, X. Zhou, Q. Zou, J. Chen, Y. Cui, P. Lin and J. Lin, Highly selective crystallization of uranium complexes for actinide partitioning in nuclear waste streams, *J. Environ. Chem. Eng.*, 2025, **13**, 120317.

[12] J. Wang, Y. Li, R. Yao, B. Yang, W. Qu, J. Lu, Z. Wu, Y. Li, Z. Lu, Z. Geng and Z. Wang, Selective Crystallization Separation of Uranium(VI) Complexes from Lanthanides, *Inorg. Chem.*, 2024, **64**, 202–212.

[13] Y. Li, H. Lu, Y. Du, J. Qiu, P. Lin and J. Lin, Highly Efficient Separation of High-Valent Actinide Ions from Lanthanides via Fractional Crystallization, *Chin. J. Struct. Chem.*, 2025, **44**, 100562.